Journal of Power Sources 205 (2012) 272–280

Contents lists available at SciVerse ScienceDirect

Journal of Power Sources

journal homepage: www.elsevier.com/locate/jpowsour

Dual-layer hollow fibres with different anode structures for micro-tubular solid oxide fuel cells

Mohd Hafiz Dzarfan Othman [1], Nicolas Droushiotis, Zhentao Wu, Geoff Kelsall, K. Li*

Department of Chemical Engineering and Chemical Technology, Imperial College London, London SW7 2AZ, United Kingdom

ARTICLE INFO

Article history:
Received 13 August 2011
Received in revised form
14 December 2011
Accepted 1 January 2012
Available online 8 January 2012

Keywords:
Micro-tubular SOFC
Dual-layer hollow fibre
Co-extrusion
Asymmetric structure
Finger-like voids

ABSTRACT

In this study, a high performance micro-tubular solid oxide fuel cell (SOFC) has been developed by depositing a multi-layer cathode onto an improved electrolyte/anode dual-layer hollow fibre fabricated via a single-step co-extrusion/co-sintering technique. The use of 0–20 wt.% of ethanol in the inner layer spinning suspension allows the control over the asymmetric structure of the Ni–CGO anode layer, i.e. finger-like voids structure covering about 50–85% of the anode layer thickness with the rest volume occupied by sponge-like structure, and at the same time affects the morphology of the CGO electrolyte layer. The presence of finger-like voids significantly facilitates the fuel gas diffusion inside the anode, and as a result, the maximum power density increases from 1.84 W m^{-2} to 2.32 W cm^{-2}, when the finger-like voids is increased from 50% to 70% of the asymmetric anode layer. However, further growth of finger-like voids, i.e. 85% of the anode layer, dramatically reduce the number of triple-phase boundary (TPB) region and conductivity in the anode, as well as the gas-tightness property of the electrolyte, which consequently decreases the maximum power density to 0.99 W cm^{-2}. Based on the results obtained, therefore, dual-layer hollow fibres with 50–70% of finger-like voids in the anode layer can be considered as the ideal structure for producing high performance micro-tubular SOFCs.

1. Introduction

The development of anode-supported micro-tubular solid oxide fuel cells (SOFCs) using nickel (Ni) as the anode catalyst has received more and more attentions recently due to a number of advantages of this configuration, such as the relatively high electrical conductivity, good catalytic activity and low material cost. Suzuki et al. [1] reported in 2006 about the successful fabrication of a Ni–cerium-gadolinium oxide (CGO) anode-supported micro-cell with the cell diameter of 0.8 mm, by using a conventional plastic mass ram extrusion/sintering technique. This cell generated the maximum power density of over 0.30 W cm^{-2} at 550 °C. As an important effort to promote gas diffusion in the anode, Suzuki et al. improved the anode structure by introducing pore former, i.e. polymethylmethacrylate beads (PMMA) [2,3]. Using the same fabrication process and materials, the maximum power density obtained by this cell was substantially increased to 1.02 W cm^{-2} and 1.29 W cm^{-2} at 550 °C and 600 °C, respectively. Apart of using Ni–CGO anode-supported system, the same research group had also reported the improvement of Ni-scandium-stabilized zirconia (ScSZ)-cerium-doped zirconia (CDZ) anode-supported SOFC performance by controlling the microstructure of an anode electrode [4]. The cell's power density enhanced approximately 450% when the anode porosity was increased from 37% to 54%. Another recent work conducted by Sammes et al. [5,6], which fabricated Ni–CGO anode support using similar ram extrusion with bigger cell diameter (1.8 mm), also achieved outstanding power output, i.e. 1.31 W cm^{-2} at 550 °C.

As one of the first several groups employing dry-jet wet extrusion technique fabricating anode support of micro-tubular SOFC, Yang et al. [7] obtained the maximum power density of 0.38 W cm^{-2} at 800 °C, using Ni-yttrium stabilized zirconia (YSZ) cermet as the anode material, with the resultant cell diameter of about 1.7 mm. Moreover, Yang et al. [8] demonstrated the advantages of impregnating the electrode catalyst into the porous anode and cathode matrixes formed during the phase inversion process. This improvement considerably increased the maximum power density to 0.78 W cm^{-2} at 800 °C.

Another significant development in fabricating anode-supported micro-tubular SOFC has been achieved by Li et al. [9–13], where a more advanced and accurately controlled dry-jet wet extrusion technique, i.e. co-extrusion process, is employed. By using this technique and followed by a co-sintering process, a cerium-gadolinium oxide (CGO)/nickel (Ni)–CGO electrolyte/anode hollow fibre (HF) has been developed in a single-step [9,10,13]. This HF distinguishes by an electrolyte outer

* Corresponding author. Tel.: +44 0207 5945676; fax: +44 0207 5945629.
E-mail address: kang.li@imperial.ac.uk (K. Li).
[1] Membrane Technology Research Centre (AMTEC), Universiti Teknologi Malaysia, 81310 Skudai, Johor, Malaysia.

0378-7753/$ – see front matter © 2012 Elsevier B.V. All rights reserved.
doi:10.1016/j.jpowsour.2012.01.002

layer of approximately 80 μm supported by an asymmetric anode inner layer with 35% finger-like voids thickness. The resultant micro-tubular cell, which also consists of a multi-layers cathode on the dual-layer HF, produced the maximum power density of 0.59 W cm^{-2} at 570 °C [11]. Further effort to reduce the thickness of the defect-free electrolyte outer layer to as thin a 10 μm resulted in the increase of the maximum power output to 1.11 W cm^{-2} at 600 °C [12,13]. Although this result has proved the potential of dual-layer HF as a support for micro-tubular SOFC, the value of power density was still slightly lower than the Suzuki's [2,3] and Sammes's [5,6] cells with a highly porous anode and a comparable electrolyte thickness.

As reported in our previous work [14], the finger-like voids structure that formed during the phase inversion process significantly enhance the gas diffusion in the anode, therefore, a further development on the structure of the electrolyte/anode dual-layer HFs for micro-tubular solid oxide fuel cells (SOFCs) has been carried out in this study. By varying the ethanol content in the inner layer spinning suspension from 0 to 20 wt.%, a series of dual-layer HFs containing finger-like voids structure that occupying approximately 50–85% of the nickel (Ni)–CGO anode thickness was successfully fabricated. The three-point bending test, gas permeation test and electrochemical measurements have been employed to investigate the effect of finger-like voids thickness on the mechanical strength, gas-tightness property and single cell performance of the dual-layer HFs, respectively.

2. Materials and experimental methods

2.1. Materials

Commercially available cerium–gadolinium oxide ($Ce_{0.9}Gd_{0.1}O_{1.95}$ or CGO), surface area 35 m^2 g^{-1}, d_{50} 0.32 μm) and nickel oxide (NiO, surface area 5 m^2 g^{-1}, d_{50} 0.55 μm) were purchased from NexTech Materials Ltd. and were used as supplied. Polyethersulfone (PESf) (Radel A-300, Ameco Performance), ethanol (VWR Prolabo) and polyethyleneglycol 30-dipolyhydroxystearate (Arlacel P135, Uniqema) were used as a polymer binder, non-solvent and dispersant, respectively. Both N-methyl-2-pyrrolidone (NMP) (HPLC grade, Rathbone) and dimethyl sulfoxide (DMSO, Sigma–Aldrich) were used as the solvents for inner and outer layer spinning suspensions, respectively, and tap water and de-ionized water were used as the external and internal coagulants, respectively. Lanthanum strontium cobalt ferrite, $La_{0.6}Sr_{0.4}Co_{0.2}Fe_{0.8}O_3$ (LSCF) (NexTech Materials Ltd., Ohio) and ethylene glycol (99+%, Acros Organic) were used as the materials for cathode slurry.

2.2. Preparation of dual-layer HF with different anode structure

The procedure of preparing the dual-layer HFs has been described in detail elsewhere [10,12], by using ball-milling technique for preparing the spinning suspension. In order to achieve dual-layer HFs with different anode structures, the non-solvent, i.e. ethanol, was added into the spinning suspension of the inner layer and the ratio of non-solvent/solvent was varied according to the one in the previous work [14]. The detailed compositions of the spinning suspensions for fabricating the dual-layer HFs with different anode structures in this study are listed in Table 1, in which the samples are named according to the ethanol content in the inner layer (anode) spinning suspension. As can also be seen in the table, different solvents were used for inner and outer layer spinning suspensions, in which NMP was for the inner and DMSO for the outer one.

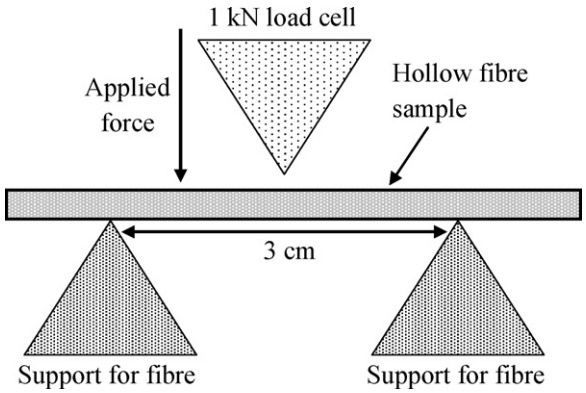

Fig. 1. Schematic representation of three-point bending strength testing apparatus.

The prepared suspensions were degassed at room temperature under stirring, loaded into two stainless steel syringes, and were simultaneously co-extruded by a syringe pump (PHD 2000 Programmable, HARVARD APPARATUS) through a triple-orifice spinneret [9] (the extrusion rates of the inner layer and the outer layer were 6 and 0.8 cm^3 min^{-1}, respectively) into a tap water coagulation bath with 20 cm air-gap length. De-ionized water was used as an internal coagulant with flow rate of 14 cm^3 min^{-1}. The HF precursors were then co-sintered by heating in air at 1500 °C for 12 h in a tubular furnace (TSH17/75/450, ELITE). The co-sintered CGO/NiO–CGO dual-layer HFs were reduced to CGO/Ni–CGO dual-layer HFs at 550 °C using pure hydrogen for 2.5 h.

2.3. Characterizations

A JEOL JSM-5610 scanning electron microscope (SEM) was used to examine the morphology of the reduced HFs. The HF samples were placed on a metal holder and sputtered by gold under vacuum. High resolution images of the cross-section of the HFs were taken at different magnifications using backscattered electrons (BSE) and secondary electron imaging (SEI) modes.

The mechanical strength of hollow fibres was examined by three-point bending test using an Instron Model 5544 tensile tester provided with a load cell of 1 kN, as illustrated in Fig. 1. Dual-layer hollow fibres were fixed on the sample holder with a 30 mm distance. The bending strength (B_F) is calculated using the following equation [15]:

$$B_F = \frac{8NLD_o}{\pi(D_o^4 - D_i^4)} \quad (1)$$

where N is the measured load at which fracture occurred (N); L, D_o, D_i are the length, the outer diameter and the inner diameter of the hollow fibres (m), respectively.

A nitrogen (N_2) gas-tightness test which has been described elsewhere [10,16] was used to determine the integrity of the outer electrolyte layer of the HFs at room temperature. The pressure change in the system over a certain period of time was monitored by a pressure gauge. The gas permeability is calculated based on the change of cylinder pressure with time, using the following equation:

$$P = \frac{V}{RT \cdot A_m t} \ln\left(\frac{p_o - p_a}{p_t - p_a}\right) \quad (2)$$

where P is the permeability of the sample (mol m^{-2} s^{-1} Pa^{-1}); V is the volume of the test cylinder (m^3); R is the gas constant (8.314 J mol^{-1} K^{-1}); T is the measured temperature (K); p_o and p_t are the initial and final measured pressures in the test cylinder (Pa); p_a is the atmospheric pressure (Pa); A_m (m^2) is the normalized membrane area and is defined as $A_m = [\pi(D_o - D_i)L]/\ln(D_o/D_i)$,

Table 1
Compositions of the spinning suspensions for dual-layer HFs with different anode structures.

Layer	Fibre	Composition (wt.%)						NMP – ethanol composition (wt.%)	Viscosity (cP)
		NiO	CGO	PESf	Arlacel P135	NMP + ethanol	DMSO		
Inner	E-0	42.00	28.00	7.00	0.12	22.88	–	100–0	19,800
	E-5							95–5	18,800
	E-10							90–10	21,400
	E-15							85–15	22,100
	E-20							80–20	22,900
Outer	E-0	–	60.00	6.00	0.12	–	33.88	–	3930
	E-5								
	E-10								
	E-15								
	E-20								

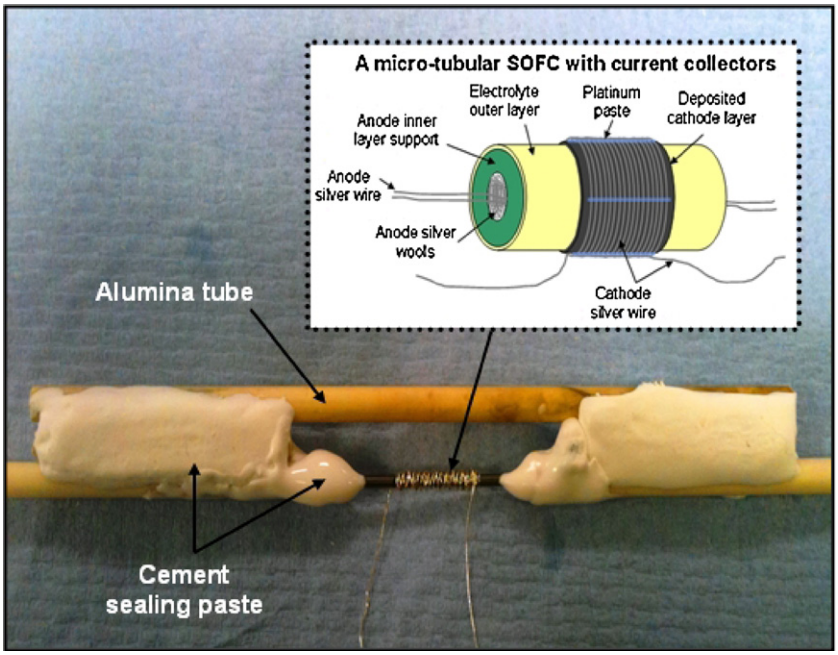

Fig. 2. Experimental apparatus of the single micro-tubular cell measurement.

where D_o and D_i are, respectively, the outer and the inner diameter of the hollow fibre (m); L is the length of the HF membrane (m); and t is the time for the test (s).

Prior to the electrochemical performance measurement, a multi-layer cathode, consists of two layers of lanthanum strontium cobalt ferrite (LSCF)-CGO (50–50 wt.%) followed by an additional layer of 100% LSCF, was coated onto the HF's electrolyte surface by brush painting technique and sintered at 1200 °C for 5 h. Both ends of the resultant micro-tubular SOFC were fixed into gas-tight aluminium tubes (Multilab Ceramics, UK) using a ceramic sealing paste (Aremco, USA) with current collectors connected to the anode and the cathode. Another alumina tube was used to strengthen the design for practical operations, which the schematic image of the reactor design is shown in Fig. 2. The complete reactor was inserted in the centre of a tube furnace (MTF 12/25/250, CARBOLITE). The electrochemical performance of the cells was measured using a potentiostat/galvanostat (Autolab® PGSTAT 30, Netherlands) at 600 °C, with a 15–30 $cm^3\,min^{-1}$ of hydrogen gas (saturated with water vapour of 0.35–0.70 $cm^3\,min^{-1}$ using a bubbling cylinder at 20 °C, 1 atm) fed to the anode and a 40 $cm^3\,min^{-1}$ (20 °C, 1 atm) of air to the cathode. The AC impedance spectra were measured on the same electrochemical workstation (0.01 Hz–1 MHz) with signal amplitude of 10 mV under open-circuit conditions at 600 °C.

3. Results and discussion

In one of our previous studies [12], a trade-off between the power output and the open-circuit voltage (OCV) of the cells was observed when the thickness of the electrolyte layer was reduced to a certain level by using the co-extrusion/co-sintering technique. As can be seen in Fig. 3, for example, there is a big difference in the maximum power outputs between the cell R-0.5 with a 10 μm electrolyte layer (outer layer extrusion rate of 0.5 $cm^3\,min^{-1}$) and the cell R-1 with a 19 μm electrolyte layer (outer layer extrusion rate of 1.0 $cm^3\,min^{-1}$). The first cell produced 1.11 W cm^{-2} while the latter one only achieved 0.77 W cm^{-2}. However, the OCV obtained for the cell R-0.5 was only 0.77 V and was enhanced to 0.85 V when the thickness of the electrolyte was increased to 19 μm for the cell R-1. In order to achieve a new batch of cells that have high values in both OCV and power output, the dual-layer hollow fibres with the electrolyte thickness between 10 and 19 μm were fabricated in this study, by employing the outer layer extrusion rate of 0.8 $cm^3\,min^{-1}$.

3.1. Macrostructure

In order to control the size of the finger-like voids in the anode layer, certain amounts of ethanol (0–20 wt.%) as a non-solvent were employed to replace NMP and are listed in Table 1. In this work,

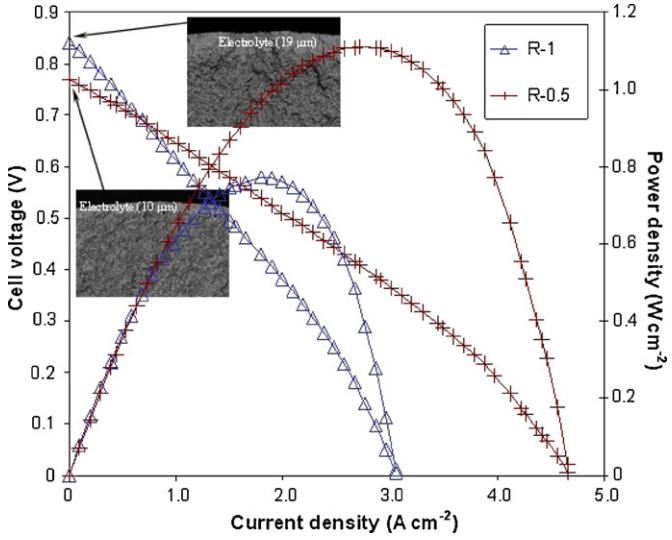

Fig. 3. *j-V* and power density curves for micro-tubular SOFC of previous batch dual-layer HFs (with 0 wt.% of ethanol in inner layer suspension) using 15 cm^3 min^{-1} of hydrogen gas [11].

NMP is used as solvent of the inner layer spinning suspension, instead of DMSO (as in batches of fibres produced in [10] and [12]). Due to the high freezing point of DMSO (i.e. 18.5 °C), the mixing of this solvent with ethanol would result in a partial solidification of DMSO and thus, reduces the potential of DMSO as a dissolving agent for the polymer binder.

Fig. 4 shows the macrostructure of the dual-layer HFs co-sintered at 1500 °C for 12 h and reduced at 550 °C for 2.5 h. As can be seen, the anode inner layer is of an asymmetric structure consisting of a finger-like voids layer and a sponge-like layer, and the finger-like voids layer becomes shorter with the increasing amount of ethanol. Dual-layer hollow fibre without ethanol in the spinning suspension, E-0, shows the longest finger-like voids occupying about 85% of the anode thickness. The addition of 5 wt.% ethanol confines the growth of finger-like voids to around 70% of the anode layer thickness. The finger-like voids length is further reduced to approximately 60%, 55% and 50% with the further increase of the ethanol content to 10 wt.%, 15 wt.% and 20 wt.%, respectively, as shown in Fig. 4.

Such change in the morphology is in good agreement with our previous study [14], and it can be explained as; firstly, the addition of ethanol, as the non-solvent, would increase the initial viscosity of a spinning suspension, as shown in Table 1, and secondly, the presence of ethanol would accelerate the precipitation of polymer binder during the phase inversion process because the polymer phase is closer to its precipitation point, and subsequently, increase the local viscosity of the nascent fibre. The viscous fingering [17], which is considered as the main phenomenon for the formation of the finger-like voids in the ceramic hollow fibres, has been limited by these two effects and as a result, confines the growth of finger-like voids in the fibres.

The outer electrolyte layer, as can be seen in Fig. 4, is well-bounded to the inner layer, although different solvents were used for preparing the spinning suspensions of the two layers. The electrolyte layer of approximately 15 μm in thickness can be achieved when the extrusion rate of 0.8 cm^3 min^{-1} was used, as shown in Fig. 5. Moreover, although finger-like voids are observed in the electrolyte layer of fibre E-0, they are nearly eliminated in the E-5 and are totally removed in the fibre E-10. As every type of HFs was fabricated using the same procedure, except for the amount of ethanol in the inner anode layer suspension, the variation in the morphology of the outer electrolyte layer should be the result of the presence of ethanol that changes the process of phase inversion. For fibre E-0, the diffusion of NMP into the outer layer, where DMSO was the solvent, contributes to the decrease in the freezing point of DMSO and slow down the precipitation of polymer binder. This results in a lower viscosity of the outer layer suspension when in contact with the external coagulation, and allows the viscous fingering phenomenon to occur, leading to the formation of finger-like voids in the electrolyte outer layer.

The use of ethanol in the inner layer spinning suspension in fibres E-5, E-10, E-15 and E-20 has caused the diffusion of a mixture of ethanol-NMP into the DMSO region. The presence of ethanol as a non-solvent seems to be more effective in speed up the polymer precipitation in DMSO, resulting in a higher viscosity of the outer layer suspension that inhibits the formation or growth of finger-like voids. Therefore, the higher the ethanol content in the inner layer suspension, the faster the precipitation of the outer layer suspension can be, until there is no finger-like voids can be formed in the outer electrolyte layer. When the content of ethanol is at or above 25 wt.%, the polymer binder in the outer layer is almost fully precipitated when in contact with the inner layer suspension (well before being immersed in the external coagulation bath), and blocks the outer orifice of the spinneret, and therefore the dual-layer HFs for the such ethanol contents cannot be achieved. This further proves the effects of ethanol (in the inner layer suspension) on changing the phase inversion process of the outer layer suspension during the co-extrusion.

3.2. Bending strength and gas-tightness property

In this study, the mechanical property of the developed dual-layer HFs was investigated by 3-point bending test. The bending strength was then calculated using Eq. (1). Fig. 6 shows the bending strength of the dual-layer HFs as a function of ethanol content in the inner layer spinning suspension. As can be seen, the bending strength increases markedly with the enhancement of the ethanol content in the inner layer suspension (from 0 wt.% to 20 wt.%). It should be noted here that, besides the size of the finger-like structure in the anode layer, the voids in the electrolyte layer also affects the bending strength of the resultant dual-layer HFs. Consequently, the fibre using 0 wt.% ethanol, which has the longest finger-like voids in the anode and contains lots of voids in the electrolyte region, shows the lowest bending strength of about 72 MPa. The bending strength increases substantially with higher amounts of ethanol in the inner layer suspension, and reaches the highest value of 245 MPa when 20 wt.% of ethanol is employed, as the formation of finger-like voids were reduced significantly in both inner and outer layers.

Besides the bending strength, the finger-like voids in the outer layer can be considered as certain sort of defect and affect the gas-tightness property of the electrolyte layer of dual-layer HFs. Fig. 7 shows the gas-tightness of the dual-layer HFs against the ethanol content in the inner layer suspension.

As can be seen, N_2 permeability is reduced with the increase of ethanol contents. The fibre using 0 wt.% ethanol shows the highest gas permeability, namely the poorest gas-tightness, of 6.4×10^{-7} mol m^{-2} s^{-1} Pa^{-1}, due to the presence of finger-like voids in the outer layer region allowing an easier transfer of N_2. The elimination of some finger-like voids in the electrolyte layer by increasing the ethanol content to 5 wt.% has significantly reduced the pathway for gas transfer and led to a sudden drop of N_2 permeability to 4.1×10^{-8} mol m^{-2} s^{-1} Pa^{-1}. The further addition of ethanol, which means a denser electrolyte layer was produced, improves the gas-tightness property of the

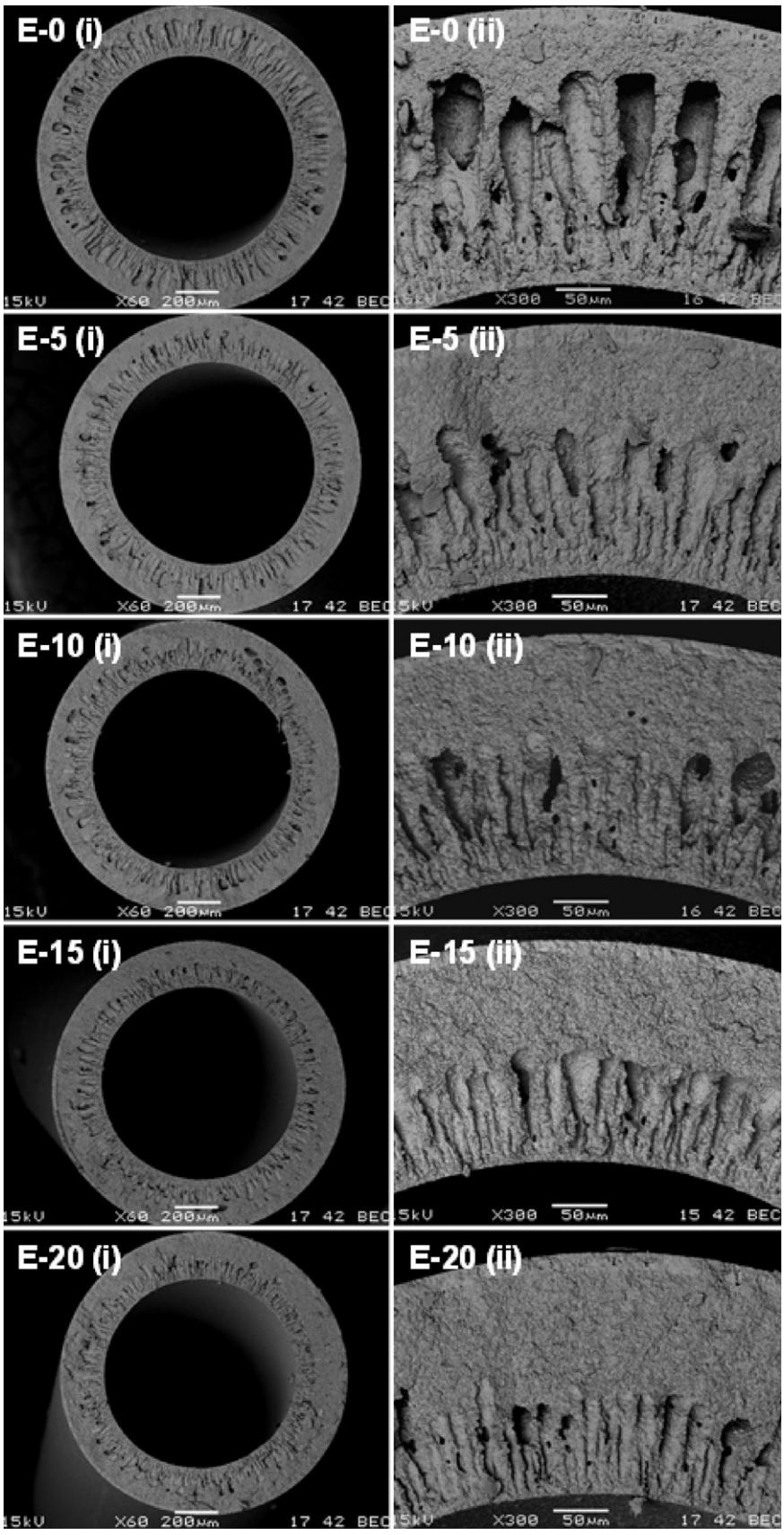

Fig. 4. EM images of the (i) overall view, and (ii) cross-section of the dual-layer HFs.

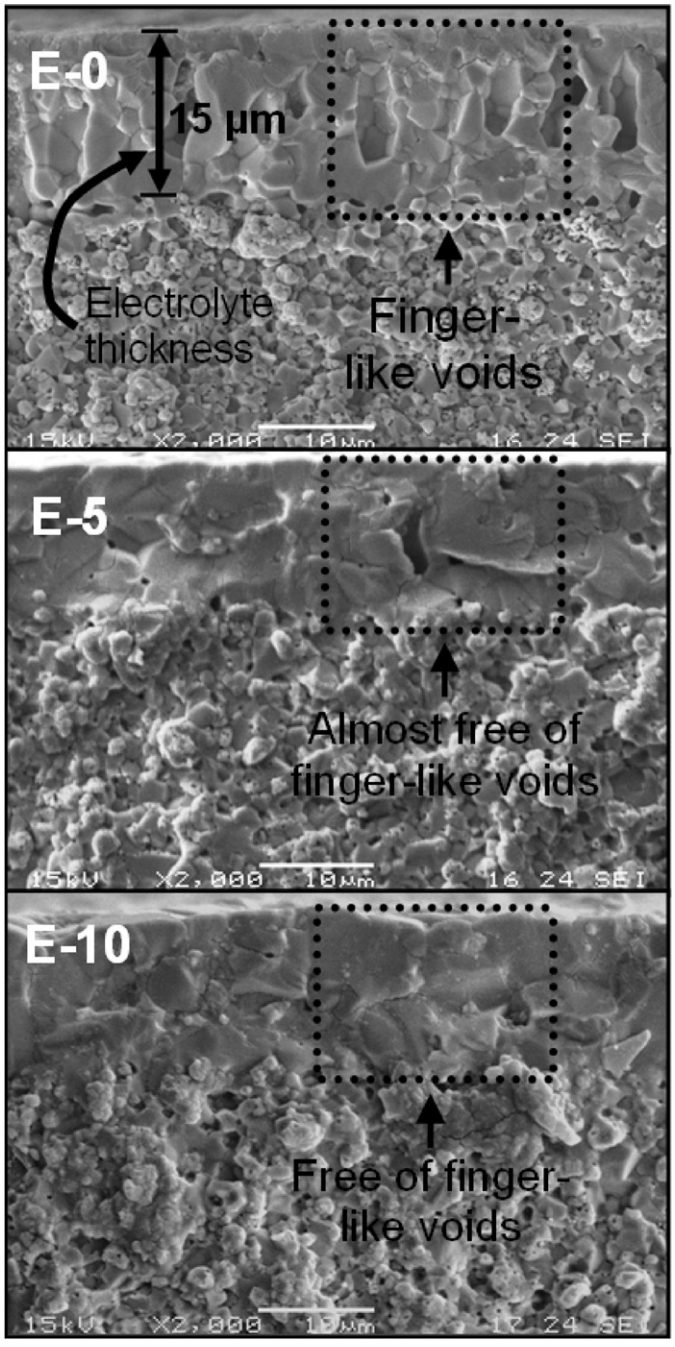

Fig. 5. SEM images of the electrolyte inner layer of the dual-layer HFs.

electrolyte by further decrease in N_2 permeability to as low as 1.2×10^{-8} mol m^{-2} s^{-1} Pa^{-1} when 20 wt.% ethanol was used.

3.3. Electrochemical performance

A multi-layer cathode consisting of two layers of LSCF-CGO cermet and one layer of pure LSCF was brush-painted onto the electrolyte layer and sintered at 1200 °C for 5 h. As can be observed in Fig. 8, the obtained cathode of approximately 40 μm is porous and uniform, which greatly facilitates gas transport and reduction reaction in the cathode. The cathode layer is also in good contact with the electrolyte surface of the dual-layer HFs.

The electrochemical performance of the full cell was investigated at 600 °C using humidified hydrogen gas at the anode (lumen side), and air at the cathode side (outer surface). Fig. 9 shows the

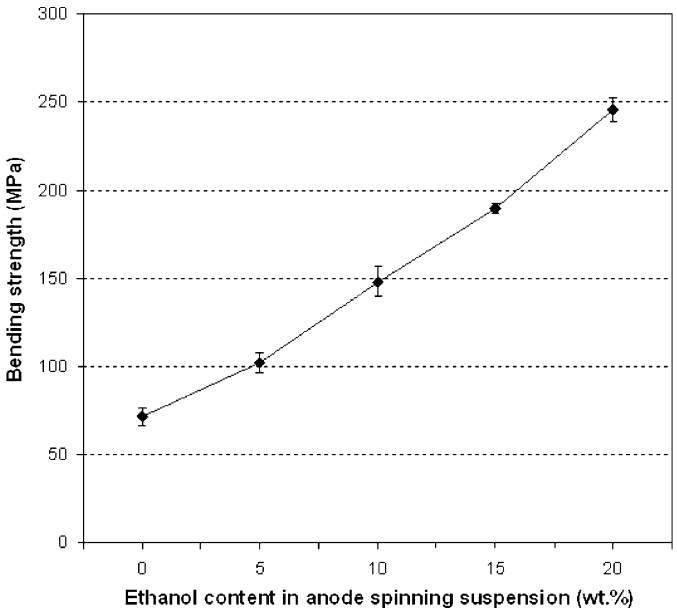

Fig. 6. Bending strength of the dual-layer HFs at different ethanol contents in the inner layer spinning suspension (number of samples = 5).

current density–voltage (j–V) and power density curves of the cell made from fibre E-20 (approximately 50% of the finger-like structure in the anode together with a 15 μm electrolyte layer) with hydrogen flow rates of 15 and 30 cm^3 min^{-1} (saturated with water vapour of 0.35 and 0.70 cm^3 min^{-1}, respectively, using a bubbling cylinder at 20 °C, 1 atm) and air flow rate of 40 cm^3 min^{-1} (20 °C, 1 atm). This cell shows an open circuit voltage (OCV) of about 0.81 V when the hydrogen flow rate is 15 cm^3 min^{-1}. This value is lower than the Nernst potential of 1.16 V at 600 °C, which is probably due to the possible minor diffusion of molecular hydrogen from the anode side to the oxidant (i.e. oxygen) region in the cathode side or vice versa, leading to the direct contact of these two gases. Furthermore, low electronic conductivity of the CGO electrolyte at the operating temperature of 600 °C, which basically created short circuit pathways, is also one of the reasons for the lower OCV.

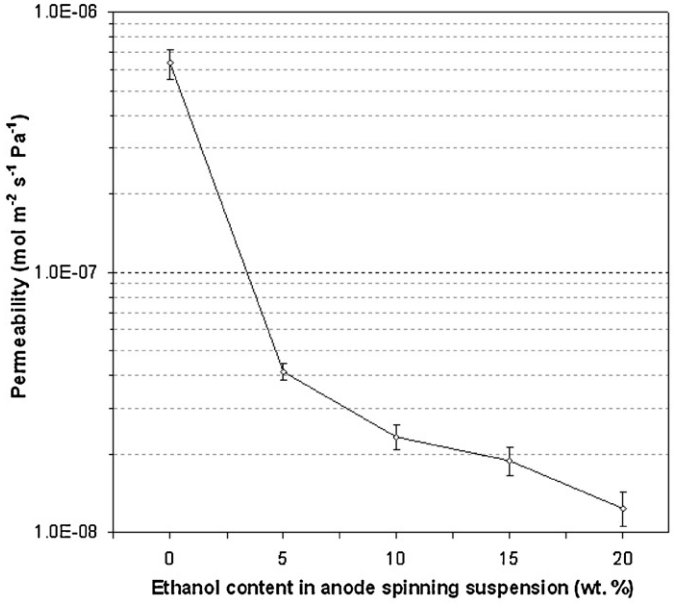

Fig. 7. Gas-tightness property as a function of ethanol content in the inner layer spinning suspension.

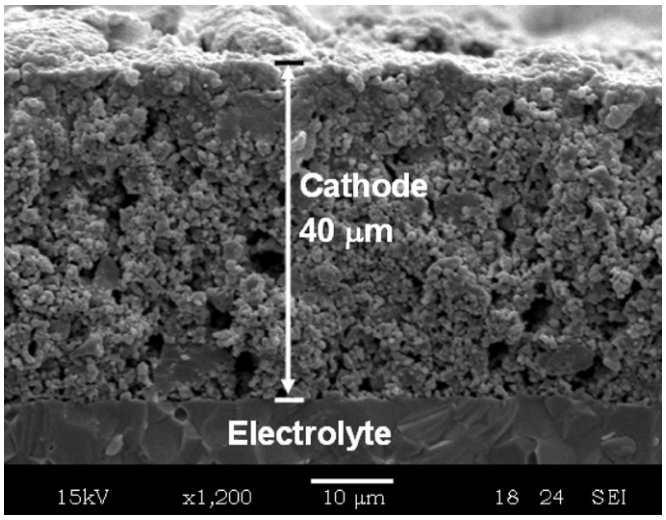

Fig. 8. Cross-sectional SEM image of the cathode layer for the micro-tubular SOFC.

Although lower than the theoretical value, the OCV value obtained in this study is in very good agreement with our previous study [12] presented in Fig. 3, in which the OCV of the cell E-20 with a 15 μm electrolyte (0.81 V) fabricated in this work is between the OCV of the cell with 10 μm electrolyte (0.77 V) and the one with 19 μm electrolyte (0.85 V). This is another evidence of the influence of electrolyte thickness on the OCV value of the cell. As can also be seen in Fig. 9, the OCV of the cell E-20 reduces to 0.79 V with the increase of the hydrogen flow rate to 30 cm^3 min^{-1}, probably due to the higher pressure in the lumen side that increases the hydrogen permeation through the electrolyte layer.

In term of the maximum power density of the cell, the E-20 produces approximately 1.25 W cm^{-2} and 1.84 W cm^{-2} when the hydrogen flow rates were 15 and 30 cm^3 min^{-1} respectively. This difference is probably due to the increase in the pressure of the lumen by increasing of the fuel flow rate and thus, enhances the driving force for the fuel to diffuse into the small pores in the sponge-like structure in the anode, where the majority of triple-phase boundary (TPB) region is located [18]. Moreover, due to the huge difference in the power density results, the hydrogen flow rate of 30 cm^3 min^{-1} was used in the following experiments.

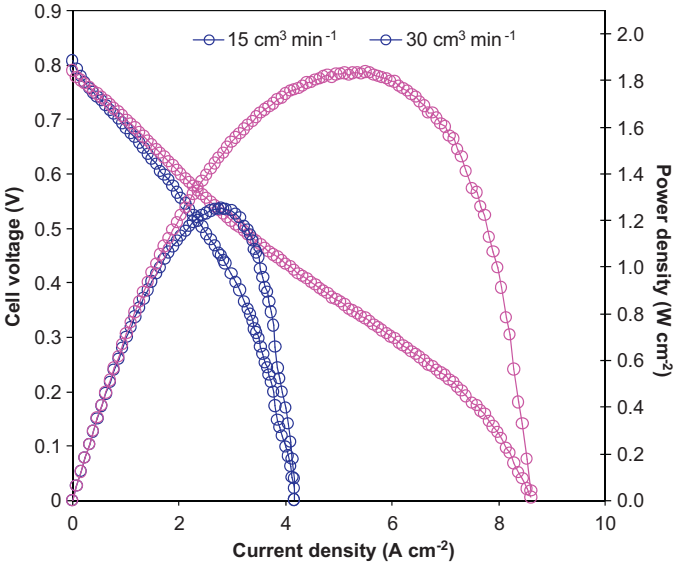

Fig. 9. *j-V* and power density curves for the micro-tubular SOFC of E-20 at flowrates of 15 and 30 cm^3 min^{-1}.

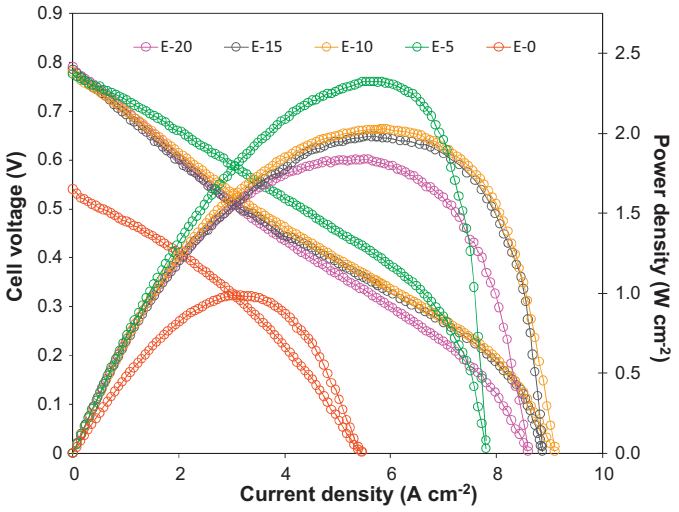

Fig. 10. *j-V* and power density curves for micro-tubular SOFCs with different anode structures at hydrogen fuel flowrate of 30 cm^3 min^{-1}.

Fig. 10 presents the results of the fuel cell test of the E-0, E-5, E-10, E-15 and E-20 at 600 °C, using 30 cm^3 min^{-1} of hydrogen. It can be seen that the cell E-0 with the longest finger-like voids in the anode shows a very low OCV of only about 0.54 V, which can be attributed to the gas leakage across the electrolyte layer due to the presence of the finger-like voids in the thin outer layer. In contrast, the cells E-5, E-10, E-15 and E-20, which possessed much better gas-tightness property (Fig. 7), show considerably higher OCV between 0.77 and 0.79 V. Although the obtained OCVs are still lower than the Nernst voltage, they are in very good agreement with the OCVs of the CGO-based micro-tubular SOFCs that were previously reported in literatures [1–6,19–24].

As also presented in Fig. 10, the power density of the cells is closely related to the anode structure. The cell E-20 with only 50% finger-like voids in the anode shows the maximum power density of 1.84 W cm^{-2}, which increases slightly to 1.98 W cm^{-2} for the cell E-15 with 55% voids structure. With the increasing sizes of the finger-like voids, the maximum power density keeps increasing to 2.03 and 2.32 W cm^{-2} for E-10 (with 60% of void thickness) and E-5 (with 70% voids thickness), respectively. As shown in our previous work [14], longer finger-like voids normally have bigger finger-like voids entrance pore, which thus results to a lower resistance of fuel gas diffusion into the finger-like voids zone. Furthermore, it has been proposed by Rahman et al. [25,26] that the conical shape of finger-like voids would create some vortex-flow inside the macro-voids. Therefore, it is believed that the presence of longer voids would enhance fuel gas mixing and subsequently facilitates better and more uniform fuel gas distribution throughout the TPB in sponge-like region, as schematically shown in Fig. 11.

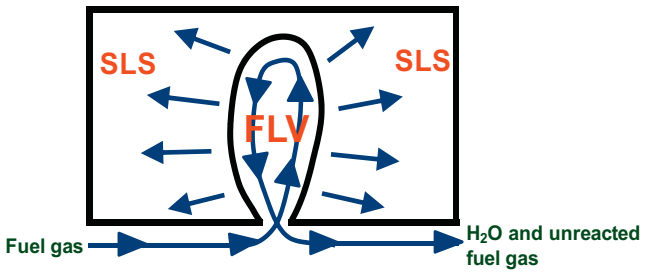

Fig. 11. Schematic representation of the predicted fuel gas diffusion in asymmetric anode inner layer (FLV: finger-like void, SLS: sponge-like structure).

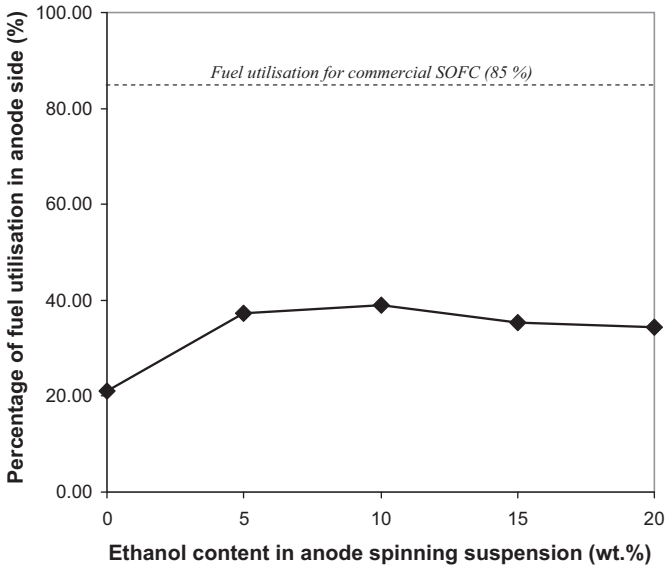

Fig. 12. Fuel utilization percentage as a function of ethanol content in the inner layer spinning suspension.

However, the finger-like voids of this type also significantly reduce the number of TPB region and conductivity of the anode. When the finger-like voids are further increased to 85% of anode thickness, i.e. the cell E-0, a big drop in the cell performance is observed and the maximum power density is only 0.99 W cm^{-2}. Moreover, the low OCV of the cell as the result of the gas diffusion across the electrolyte is also one of the main reasons for the low electrochemical performance. In comparison with other studies on micro-tubular SOFCs, four out of five cells developed in this study, i.e. E-5, E-10, E-15 and E-20, show very outstanding performances and their maximum power densities at 600 °C are considerably higher than the ones reported by Suzuki et al. [3] and Sammes et al. [5,6], which further demonstrates the advantages of the co-extrusion and co-sintering process in fabricating dual-layer HFs and in optimizing HF structure for better cell performance.

Fig. 12 shows the fuel utilization in the anode as a function of ethanol content in the inner layer spinning suspension. The fuel utilization (U_f) has been computed using Eq. (3) as shown below [27]:

$$U_f = \frac{I}{2F \times n_{H_2,inlet}} \times 100\% \quad (3)$$

where I is the electric current provided by the cell (A), F is the Faraday constant (As mol^{-1}) and $n_{H_2,inlet}$ is the hydrogen molar flow rate provided to the cell (mol s^{-1}). The current value in this study is referred to the current at the maximum power density, based on the assumption that the electric current is a linear function of the molar flow of the spent fuel [28].

As can be seen, the cell E-0 that using 0 wt.% ethanol shows the lowest fuel utilization in the anode of only about 21.2%. The reasons for this are similar to the one for the lowest maximum power density achieved by this cell, i.e. possible gas diffusion across the electrolyte and less TPB area in the anode. While much higher fuel utilizations between 34.5 and 38.9% can be achieved for E-5 to E20. However, the fuel utilization of the cells obtained in this study is still considerably low when compared to the fuel utilization level of the commercial fuel cell (about 85%) [29].

In order for a clearer understand on the resistance of each component of the cells, an impedance analysis has been carried out. Fig. 13(a) shows impedance analysis for the micro-tubular SOFCs at 600 °C to determine the relative area specific resistance (ASR) of the

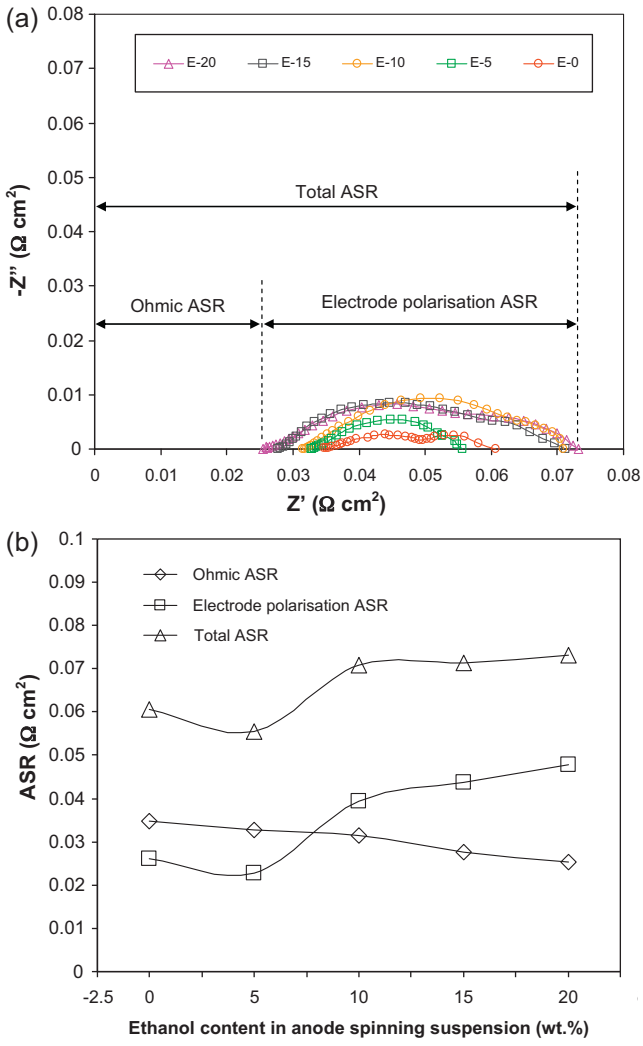

Fig. 13. (a) Impedance spectra of the cells with different anode structures; (b) the ASR as a function of ethanol content in the inner layer spinning suspension.

cells. According to Mogensen and Hendriksen [30], total ASR may be divided into ohmic ASR and electrode polarisation ASR. As shown in the graph, the distance from first intercept to the zero value on the real impedance axis represents the ohmic ASR in the cell, while the distance between second and first intercepts shows the electrode polarisation ASR. In order to study the effect of cell macrostructures on the cell resistances, the values of ohmic ASR, electrode polarisation ASR and total ASR obtained from this graph were then employed to plot the graph of ASR against the ethanol content in the inner layer spinning suspension as presented in Fig. 13(b).

As can be seen in Fig. 13(b), the ohmic ASR of the cells reduces slightly with the addition of ethanol in the inner layer spinning suspension. According to Mogensen and Hendriksen [30], the ohmic ASR originates from the electrolyte, the electrode materials and the current collection arrangement. As the current collector and cathode in this study were built in a similar way for each cell, it can be assumed that the effects of current collection and cathode on the ohmic ASR are almost negligible. Meanwhile, the ohmic ASR from the electrolyte is much higher than the one in the anode [31] and therefore, the different anode structure does not greatly affect the total ohmic ASR value, and it is believed that the trend of the ohmic ASR that obtained in this study is largely resulted from the difference in the electrolyte structure. Thus, the reduction of the macro-voids in the electrolyte layer by the

presence of higher ethanol content in the inner layer spinning suspension has increased the conductivity of the electrolyte and consequently reduces the ohmic ASR of the cells.

For the electrode polarisation ASR, it represents several types of resistances [30] such as the resistance from the gas phase diffusion, and the resistance due to gas conversion, i.e. fuel oxidation and oxygen reduction. Based on this understanding, it is strongly believed that the variation in the anode structure would affect very much the value of the electrode polarisation ASR. As can be seen in Fig. 13(b), the electrode polarisation ASR is decreased with the increase of ethanol content from 0 wt.% to 5 wt.%, probably due to the smaller TPB region that results to the less fuel oxidation reaction of the cell that using 0 wt.% ethanol (85% finger-like voids thickness) compared to the cell that using 5 wt.% ethanol (70% in thickness). However, the resistance from the fuel gas diffusion in the anode seems to be more dominant for the cell with finger-like voids thickness of 60%, 55% and 50%, which fabricated from 10 wt.%, 15 wt.% and 20 wt.% of ethanol in the inner layer suspension since the value of electrode polarisation ASR of the cells increases as a function of ethanol content. This shows that the finger-like voids are really beneficial in promoting the gas diffusion in the anode and subsequently, minimises the electrode polarisation ASR in the cell.

In addition, the line of total ASR as a function of ethanol content is almost similar to the electrode polarisation ASR trend, and this indeed shows that, the difference in the anode structure in this study has bigger effect on the cell performance than the electrolyte ohmic ASR. In comparison to other cells reported in previous works [1,2,5,6,8,12,32,33], the resistances of the cells in this study are much lower and thus, explaining the outstanding power outputs of the obtained cells.

4. Conclusions

A set of dual-layer hollow fibres (HFs) with 50–85% of the finger-like voids thickness in the anode inner layer has been successfully fabricated, by varying the ethanol content in the inner layer spinning suspension from 0 to 20 wt.%. The use of ethanol in the inner layer spinning suspension not only affects the structure of the anode, but also the structure of the electrolyte, due to the formation of macro-voids in the outer layer when lesser ethanol was used. The difference in the structures in both inner and outer layers of the dual-layer HFs give big impact to the bending strength of the fibres, while the gas-tightness property of the HFs is only affected by the outer layer. In term of electrochemical performance, the maximum power density of the cells fabricated in this study varies with the anode structure. The bigger finger-like voids entrance pore size in the anode with longer finger-like voids would results in a lower resistance of fuel gas diffusion into the finger-like voids zone. It is also believed that the finger-like voids structure in the anode act as a set of hundreds micro-channels that improve the fuel mixing and diffusion in the anode triple-phase boundary (TPB) region. Therefore, it is discovered that the maximum power density increases significantly with the increase of finger-like voids thickness and reaches the highest value at 2.32 W cm^{-2} for the cell with 70% finger-like voids thickness. However, at a certain point, the finger-like voids also markedly reduce the number of TPB region and conductivity of the anode, and thus, affecting the overall cell performance. This study also proves that the structure of the anode has huge impact to the resistance of the cells and suggests that the anode structure is one of the major parameters that have to be considered in order to produce a high performance micro-tubular SOFC.

Acknowledgements

The authors gratefully acknowledge the research funding provided by EPSRC (EP/E00136X) in the United Kingdom. The award of an overseas study bursary to MHDO by the Malaysian Ministry of Higher Education (MoHE) and Universiti Teknologi Malaysia (UTM) is also gratefully acknowledged.

References

[1] T. Suzuki, T. Yamaguchi, Y. Fujishiro, M. Awano, Journal of Power Sources 160 (2006) 73–77.
[2] T. Suzuki, Y. Funahashi, T. Yamaguchi, Y. Fujishiro, M. Awano, Solid State Ionics 180 (2009) 546–549.
[3] T. Suzuki, Y. Funahashi, T. Yamaguchi, Y. Fujishiro, M. Awano, in: T.S. Zhao (Ed.), Micro Fuel Cells – Principles and Applications, Elsevier, Oxford, UK, 2009, pp. 141–177.
[4] T. Suzuki, Z. Hasan, Y. Funahashi, T. Yamaguchi, Y. Fujishiro, M. Awano, Science 325 (2009) 852–855.
[5] F. Calise, G. Restucccia, N. Sammes, Journal of Power Sources 195 (2010) 1163–1170.
[6] Y.W. Sin, K. Galloway, B. Roy, N.M. Sammes, J.H. Song, T. Suzuki, M. Awano, International Journal of Hydrogen Energy 36 (2011) 1882–1889.
[7] C. Yang, W. Li, S. Zhang, L. Bi, R. Peng, C. Chen, W. Liu, Journal of Power Sources 187 (2009) 90–92.
[8] C. Yang, C. Jin, F. Chen, Electrochemistry Communications 12 (2010) 657–660.
[9] N. Droushiotis, M.H.D. Othman, U. Doraswami, Z. Wu, G. Kelsall, K. Li, Electrochemistry Communications 11 (2009) 1799–1802.
[10] M.H.D. Othman, Z. Wu, N. Droushiotis, U. Doraswami, G. Kelsall, K. Li, Journal of Membrane Science 351 (2010) 196–204.
[11] N. Droushiotis, U. Doraswami, D. Ivey, M.H.D. Othman, K. Li, G. Kelsall, Electrochemistry Communications 12 (2010) 792–795.
[12] M.H.D. Othman, N. Droushiotis, Z. Wu, K. Kanawka, G. Kelsall, K. Li, Journal of Membrane Science 365 (2010) 382–388.
[13] M.H.D. Othman, N. Droushiotis, Z. Wu, G. Kelsall, K. Li, Journal of Power Sources 196 (2011) 5035–5044.
[14] M.H.D. Othman, Z. Wu, N. Droushiotis, G. Kelsall, K. Li, Journal of Membrane Science 360 (2010) 410–417.
[15] S. Liu, K. Li, R. Hughes, Ceramics International 29 (2003) 875.
[16] X. Tan, Y. Liu, K. Li, AIChE Journal 51 (2005) 1991.
[17] B.F.K. Kingsbury, K. Li, Journal of Membrane Science 328 (2009) 134.
[18] U. Doraswami, P. Shearing, N. Droushiotis, K. Li, N.P. Brandon, G.H. Kelsall, Solid State Ionics 192 (2011) 494–500.
[19] T. Suzuki, T. Yamaguchi, Y. Fujishiro, M. Awano, Journal of The Electrochemical Society 153 (2006) A925–A928.
[20] Y. Liu, S.I. Hashimoto, H. Nishino, K. Takei, M. Mori, T. Suzuki, Y. Funahashi, Journal of Power Sources 174 (2007) 95–102.
[21] T. Yamaguchi, T. Suzuki, S. Shimizu, Y. Fujishiro, M. Awano, Journal of Membrane Science 300 (2007) 45–50.
[22] T. Suzuki, Y. Funahashi, Z. Hasan, T. Yamaguchi, Y. Fujishiro, M. Awano, Electrochemistry Communications 10 (2008) 1563–1566.
[23] V. Gil, J. Gurauskis, R. Campana, R.I. Merino, A. Larrea, V.M. Orera, Journal of Power Sources 196 (2011) 1184–1190.
[24] F. Calise, G. Restucccia, N. Sammes, Journal of Power Sources 196 (2011) 301–312.
[25] M.A. Rahman, F.R. García-García, M.D. Irfan Hatim, B.F.K. Kingsbury, K. Li, Journal of Membrane Science 368 (2011) 116–123.
[26] M.A. Rahman, Catalytic hollow fibre membrane micro-reactors for energy applications, Ph.D thesis, Imperial College London, UK, 2011.
[27] N.M. Sammes, Y. Du, R. Bove, Journal of Power Sources 145 (2005) 428–434.
[28] W. Winkler, in: S.C. Singhal, K. Kendall (Eds.), Thermodynamics, in High-Temperature Solid Oxide Fuel Cells: Fundamentals, Design and Applications, Elsevier, Oxford, UK, 2003, pp. 53–82.
[29] R.J.F. Gerwen, in: S.C. Singhal, K. Kendall (Eds.), Systems and Applications, in High-Temperature Solid Oxide Fuel Cells: Fundamentals, Design and Applications, Elsevier, Oxford, UK, 2003, pp. 363–392.
[30] M. Mogensen, P. Hendriksen, in: S.C. Singhal, K. Kendall (Eds.), Testing of Electrodes, Cells and Short Stacks, in High-Temperature Solid Oxide Fuel Cells: Fundamentals, Design and Applications, Elsevier, Oxford, UK, 2003, pp. 261–289.
[31] E. Ivers-Tiffée, A.V. Virkar, in: S.C. Singhal, K. Kendall (Eds.), Electrode Polarisations, in High-Temperature Solid Oxide Fuel Cells: Fundamentals, Design and Applications, Elsevier, Oxford, UK, 2003, pp. 229–260.
[32] C. Yang, C. Jin, F. Chen, Electrochimica Acta 56 (2010) 80–84.
[33] F. Zhao, C. Jin, C. Yang, S. Wang, F. Chen, Journal of Power Sources 196 (2011) 688–691.